

Magnetotransport in bundles of intercalated carbon nanotubes

M. Baxendale,* V. Z. Mordkovich, and S. Yoshimura

Yoshimura π -Electron Materials Project, ERATO, JRDC, c/o Matsushita R.I.T., Incorporated, Tamu-ku, Kawasaki 214, Japan

R. P. H. Chang

Materials Research Center, Northwestern University, Evanston, Illinois 60208

(Received 27 September 1996; revised manuscript received 27 January 1997)

Two types of quantum magnetotransport behavior were observed in pristine bundles of helicoidal carbon nanotubes. Universal conductance fluctuations for $T < 10$ K and an underlying positive magnetoconductance to very high magnetic fields for $T < 100$ K are the most notable features of one of these types. Remarkably, this behavior was observed after intercalation of potassium guest atoms into pristine bundles of the other type. This range of phenomena is explained within the theory of weak localization and interaction effect in three dimensions. However, the observed inelastic scattering mechanism for K-intercalated bundles cannot be described by the present theory for a common mechanism of the same dimensionality. [S0163-1829(97)03828-9]

I. INTRODUCTION

There have been several recent reports of electrical measurements performed on a single multiwall carbon nanotube announcing many interesting properties including large jumps in resistivity over a narrow temperature range and universal conductance fluctuations.^{1,2} However, the experimental difficulties encountered are considerable. In this paper we report the magnetotransport properties of macroscopic bundles of closely packed multiwall nanotubes successfully intercalated with guest atoms of potassium without breaking the tubular structure.³ The success of the intercalation process is indirect evidence that the nanotubes are helicoidal rather than the closed Russian doll type.³ The advantage of this approach is that it allows measurements to be performed on the same bundle in the pristine and intercalated states and facilitates the handling of active K-intercalated samples. These measurements elucidate the gross effects of K intercalation rather than modification of the electronic structure of individual nanotubes.

The nanotube bundles used in this study were produced by one of the authors by arc discharge in a He atmosphere as described elsewhere.⁴ Transmission electron microscopy studies confirm that the material comprises defectless, aligned multiwall nanotubes close packed into bundles of outer diameter several tens of nanometers.⁴ These bundles in turn form bigger fiberlike structures of length 1–3 mm and approximate diameter 0.1 mm (i.e., an ensemble of 10^{10} – 10^{12} individual multiwall nanotubes). These structures were used as the host material for intercalation.

Song *et al.* have reported the galvanometric properties of similar pristine bundles produced by one of the authors; these can be summarized as (i) $T > 60$ K, p -type semimetallic behavior consistent with the simple two-band model for semimetallic graphite; (ii) low-temperature properties partially described by two-dimensional (2D) weak localization (WL) theory.⁵ We also observed these properties for the majority of samples (labeled type I) taken from the growth on the cathode used in the arc discharge method. However, a minority of samples (labeled type II) exhibited a dramati-

cally different behavior: (i) conductance, $G(T)$, in the range 2–300 K is 10^1 – 10^2 lower than that of similar-sized type-I samples; (ii) appearance of random magnetoconductance fluctuations for $T < 10$ K; and (iii) a large underlying positive magnetoconductance to very high fields for $T < 100$ K.

It is remarkable that K intercalation of a type-I pristine material produced nanotube bundles that exhibit the type-II behavior. In this paper we report this range of phenomena can be described within the framework of the theory of WL and interaction effect in 3D.⁶

II. EXPERIMENT

Full details of the intercalation of potassium and other guest atoms into nanotube bundles are given elsewhere.³ Scanning electron microscope studies revealed a dramatic change in the appearance of individual nanotubes. Straight pristine nanotubes are transformed after intercalation into a “bead-line” pattern comprising swollen intercalated sections and narrow nonintercalated “necks” (K guest atoms are prevented from propagating along the length of the nanotubes by defects in the graphene helicoid), Fig. 1. The appearance of this characteristic pattern can only be explained in terms of the helicoidal model for multiwall carbon nanotubes.³ A diffraction pattern similar to that for the corresponding stage-1 graphite intercalation compound (GIC), C_8K , was observed after intercalation from which we calculate that the intershell distance increases from 3.44 to 5.3 Å.^{3,7}

Magnetotransport measurements were performed with a standard two-contact technique with the magnetic field B applied perpendicular to the sample axis. The K-intercalated sample was protected against contact with air while transferring from the inert atmosphere to the cold arm of a superconducting magnet system. Measurements were performed on the same nanotube bundle before and after intercalation.

III. RESULTS AND DISCUSSION

Figure 2 shows that the conductance variation of both the pristine and intercalated states increases with temperature. It

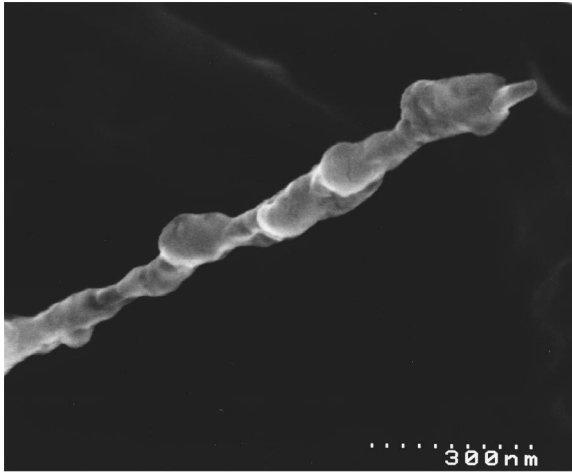


FIG. 1. Scanning electron micrograph of a K-intercalated nanotube showing the characteristic bead-line pattern.

is remarkable that for the entire temperature range conductance is lowered by K intercalation. The in-plane conductivity of C_8K is $\sim 10^4$ times higher than that of the host graphite.⁷ The introduction of disorder and/or a weakening of intertube couplings rather than a decrease in conductivity of the individual nanotubes themselves is the probable cause of this behavior.

Conductance behavior, and that of the magnetoconductance, is in qualitative agreement with the characteristics of type-II pristine nanotube bundles described above. The temperature variation for both pristine and K-intercalated states is rather weak implying intertube coupling is sufficiently strong to exclude a hopping mechanism. The conductance variation of the intercalated nanotube bundles signals 3D WL behavior, Eq. (1).⁶ For the K-intercalated nanotube bundle, the signal became time dependent at temperatures close to room temperature perhaps due to rearrangement of the intercalant.

WL effects result from the constructive interference of partially backscattered electron waves traveling back along time-reversed paths.⁶ WL effects therefore reduce conductivity. A mechanism that destroys the phase coherence of the electron, such as an inelastic scattering event or scattering at

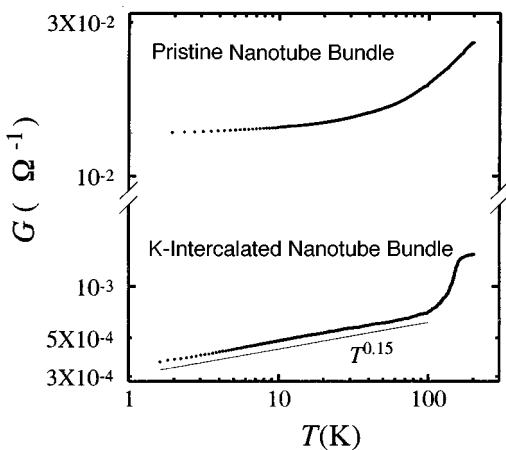


FIG. 2. Conductance vs temperature for a nanotube bundle before and after K intercalation.

a magnetic impurity, therefore quenches WL effects. Since the inelastic scattering time $\tau_{in}(T) \propto T^{-p}$, where p depends on the dominant scattering mechanism, WL effects are observed at low temperature when τ_{in} is much greater than the temperature-independent elastic scattering time τ . In perfect periodic potentials, at low temperature ($T < 5$ K) $\tau_{in} \propto T^{-2}$ for the electron-electron scattering mechanism and at higher temperatures when the electron-phonon interaction dominates, $\tau_{in} \propto T^{-3}$. Electron-electron scattering is enhanced in the presence of disorder, in 3D, $p = \frac{3}{2}$;⁸ 2D, $p = 1$; and 1D, $p = \frac{2}{3}$.⁹

In 3D, the spatial extent of phase coherence, the phase coherence length $l_\phi = \sqrt{3D\tau_\phi}$, where D is the elastic diffusion coefficient and τ_ϕ is the coherence time.⁶ Coherence time conveys the effect of inelastic and magnetic impurity scattering via $\tau_\phi(T)^{-1} = \tau_{in}(T)^{-1} + \tau_s^{-1}$, where τ_s is the magnetic scattering time; hence $l_\phi(T) = aT^{-p/2}$. Here, since the material has been shown to be of ultrahigh purity, spin scattering is neglected.⁴ In 3D, the conductivity due to WL is given by⁶

$$\sigma_{WL}(T) = \sigma_0 + \frac{e^2}{\hbar \pi^3} \frac{1}{a} T^{p/2}. \quad (1)$$

For the intercalated sample $G_{WL} \propto T^{0.15}$, i.e., $p = 0.30$, indicating that none of the inelastic scattering mechanisms outlined above are applicable. Possibly an anomalous situation in which the localization is 3D and the scattering process is disorder-enhanced 1D, as has been observed in Bi wires by Beutler and Giordano, is present.¹⁰ Either possibility implies that these processes are still not fully understood.

The theory of magnetoconductivity change, $\Delta\sigma = \sigma(B, T) - \sigma(0, T)$, due to 3D WL was formulated by Kawabata,¹¹

$$\Delta\sigma(B, T) = -\Delta\sigma_n(B) + \Delta\sigma_{WL}(B, T). \quad (2)$$

Here $\Delta\sigma_n = \sigma_0(\omega_c\tau)^2 \propto B^2$ is the ‘‘normal’’ negative component, where $\omega_c = eB/m^*$ and $\sigma_0 = ne^2\tau/m^*$ (symbols have their usual meanings).¹² The positive WL contribution,

$$\Delta\sigma_{WL}(B, T) = \frac{e^2}{2\pi^2\hbar l_B} F(\delta), \quad (3)$$

where the magnetic length $l_B = \sqrt{\hbar/eB}$. The function $F(\delta)$, where $\delta = 3l_B^2/4ll_{in}$, inelastic scattering length $l_{in} = \sqrt{3D\tau_{in}}$ and elastic scattering length $l = \sqrt{3D\tau}$, has two limits for which an analytical solution of the form $\Delta\sigma_{WL} \propto B^n$ exists,

$$\Delta\sigma_{WL}(B) = 2.9 \times 10^4 \sqrt{B} \Omega^{-1} \text{cm}^{-1} \quad (B \text{ in T}) \quad \text{for } \delta \ll 1 \quad (4)$$

and

$$\Delta\sigma_{WL}(B, T) = \sigma_0(\lambda_{in}/\lambda)^{3/2} (\omega_c\tau)^2 / 12\sqrt{3} \propto T^{-3p/4} B^2 \quad \text{for } \delta \gg 1. \quad (5)$$

Note that Eq. (4) is independent of system parameters, a form unique to 3D WL. The quantity $\delta \propto T^{p/2}/B$, hence the condition $\delta \ll 1$, is observed for high fields at low temperature. When $l_B \approx l$, the positive WL component $\Delta\sigma_{WL}$ will tend to saturate and the negative normal component $\Delta\sigma_n$

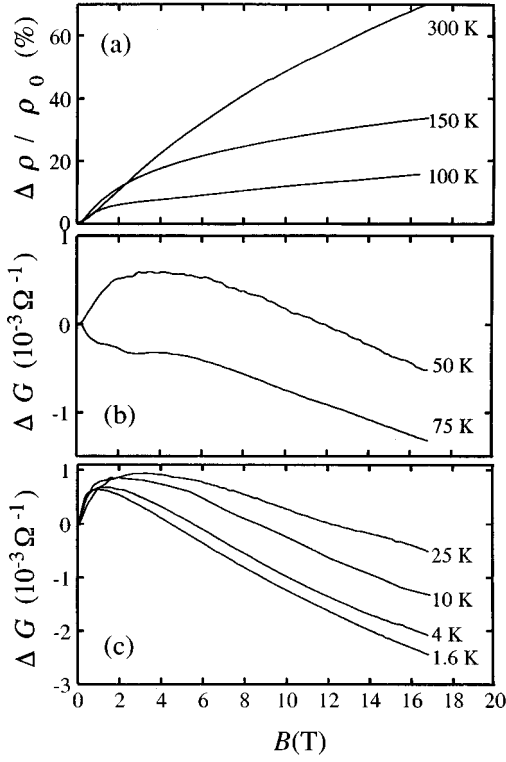


FIG. 3. Temperature variation of magnetotransport parameters for the pristine nanotube bundle showing three distinct temperature regimes: (a) 100–300 K, (b) 50–100 K, (c) 1.6–50 K.

dominate.¹¹ Hence the condition for observation of the unique temperature-independent $\Delta\sigma_{\text{WL}} \propto \sqrt{B}$ expressed in Eq. (4) can be written $l < l_B \ll \sqrt{l_{\text{in}}}$.¹¹

Magnetotransport parameters vs B at various temperatures for the pristine nanotube bundle are given in Fig. 3. In agreement with the report of Song *et al.*, three distinct temperature regimes were identified.⁵ For $T > 90$ K, magnetoresistance $\Delta\rho/\rho_0$ [$\Delta\rho = \rho(B) - \rho_0$] is a classical effect described by an angularly averaged simple two-band model.¹³ Following the procedure of Song *et al.*, curve fitting reveals the ratio of hole to electron conductivities, σ_p/σ_e , to be increasing with decreasing temperature in this regime. According to this model, as $\sigma_p/\sigma_e \rightarrow \infty$, $\Delta\rho/\rho_0 \rightarrow 0$ hence changes in low-temperature magnetotransport parameters are due to quantum phenomena, i.e., due to WL and interaction effects (these are most conveniently described in terms of $\Delta\sigma$).^{5,6,11}

The interaction effect or splitting of electron energies into spin-up and spin-down bands when the condition $h = g\mu_B B/k_B T \gg 1$ is satisfied (where g is the g factor, μ_B the Bohr magneton, and k_B the Boltzmann constant) is characterized by a conductivity change comprising two terms: $\Delta\sigma_1(B, T) = \Delta\sigma_1'(T) + \Delta\sigma_1''(B)$. The actual forms of $\Delta\sigma_1'(T)$ and $\Delta\sigma_1''(B)$ are nontrivial and $\Delta\sigma_1''(B)$ can be either positive or negative; the reader should refer to Ref. 14 for full expressions. In 3D the effect is often manifested as $\Delta\sigma_1'(T) \propto \sqrt{T}$ and $\Delta\sigma_1''(B) \propto -\sqrt{B}$ for $h \gg 1$ or $\Delta\sigma_1'(T) \propto -B^2$ for $h \gg 1$.⁶ In real systems the zero-field WL term, Eq. (1), and $\Delta\sigma_1'(T)$ are both present; to the lowest order they are believed to be simply additive.⁶

The qualitative agreement with Eq. (2) is clearly seen in the low-temperature variation of $\Delta\sigma$, Fig. 3(c). However, the observation of a temperature-dependent negative component at high fields cannot be described by WL effects alone because both $\Delta\sigma_n$ and $\Delta\sigma_{\text{WL}}$ for $\delta \ll 1$ (i.e., for high fields and low temperatures) are temperature independent. Note that $\Delta\sigma$ remains relatively unchanged in the temperature range 25–50 K suggesting that the temperature-dependent negative term is not significant for $T > 25$ K, i.e., $\Delta\sigma = -\Delta\sigma_n + \Delta\sigma_{\text{WL}}$ for $25 \text{ K} < T < 50 \text{ K}$. [In Fig. 3, for $T < 50$ K, the $\Delta\sigma_{\text{WL}} \propto B^2$ dependence of the temperature-dependent $\delta \gg 1$ limit, Eq. (5), is observed for $B \leq 0.1$ T, therefore $\Delta\sigma_{\text{WL}}$ is in the $\delta \ll 1$ limit or tending to saturate for most of the field range.] The maximum in $-\Delta\sigma_n + \Delta\sigma_{\text{WL}}$ at $B \approx 3$ T occurs when $l_B \approx l$, hence $l \approx 10$ nm for the pristine nanotube bundle; accurate curve fitting for higher fields is not possible because $\Delta\sigma_{\text{WL}}$ tends to saturate.

At $T \approx 75$ K both the WL and classical contributions to magnetotransport are evident, Fig. 3(b). For 75–100 K, $\Delta\sigma_{\text{WL}}$ collapses, indicating that the transition from $\delta \ll 1$ to $\delta \gg 1$ occurs in this temperature range.

Subtraction of $-\Delta\sigma_n + \Delta\sigma_{\text{WL}}$ from $\Delta\sigma$ ($T < 25$ K) reveals a negative term with the \sqrt{B} and \sqrt{T} dependencies at high field (i.e., $h \gg 1$; if $g = 2$ and $T = 4$ K, $h = 1$ at $B \approx 1$ T) of the 3D interaction effect.¹⁴ Hence for $T < 50$ K, the magnetotransport of the pristine nanotube bundle can be qualitatively described by the 3D WL and interaction effects.

Dramatic changes in magnetotransport behavior after K intercalation were observed, Fig. 4. Random fluctuations about a positive underlying magnetoconductance were observed to very high fields for $T < 10$ K, Fig. 4(c). In the range $10 \text{ K} < T < 100 \text{ K}$, the positive magnetoconductance collapses with temperature and at $T \approx 200$ K a small two-band-type magnetoresistance is seen, Fig. 4(a). This behavior of the underlying magnetoconductance can be described in terms of 3D WL theory, Eqs. (1)–(5), but no saturation of ΔG is observed in the field range employed, therefore $l \leq 1$ nm. The observed collapse of positive magnetoconductance is simply the transition of $\Delta\sigma_{\text{WL}}$ from the $\delta \ll 1$ to the $\delta \gg 1$ limit. For $T < 10$ K, $\Delta\sigma_{\text{WL}}$ is in the system-independent $\delta \ll 1$ limit for most of the field sweep ($\Delta\sigma \propto B^2$ for $B < 0.1$ T indicating the field range of the $\delta \gg 1$ limit and that the interaction effect is weak in this case) and far from saturation. Hence an expression embracing the field and temperature dependencies of Eq. (2), 3D interaction effect (assuming the $h \gg 1$ limit for most of the field sweep), and $\Delta\sigma_n$ was fitted to the $T < 10$ K magnetoconductance data. The result is given in Fig. 4(c) (the justification for fitting such a curve to a characteristic that exhibits random oscillations is that integrated areas above and below the smooth curve should be equal provided the field range is sufficiently high).

Since $\Delta\sigma_{\text{WL}} = f\Delta G_{\text{WL}}$, where f contains the sample dimensions and a filling factor, we calculate $f = 2 \times 10^5 \text{ cm}^{-1}$ via the temperature-independent coefficient of \sqrt{B} obtained from the above curve fitting procedure and Eq. (4). This value is equivalent to the approximate sample dimensions with a filling factor of 25%. Thus the absolute value of conductivity of the K-intercalated nanotube bundle in the range $2 \text{ K} < T < 200 \text{ K}$ is $10\text{--}10^2 \text{ } \Omega^{-1} \text{ cm}^{-1}$. There are several possible reasons why the filling factor is less than

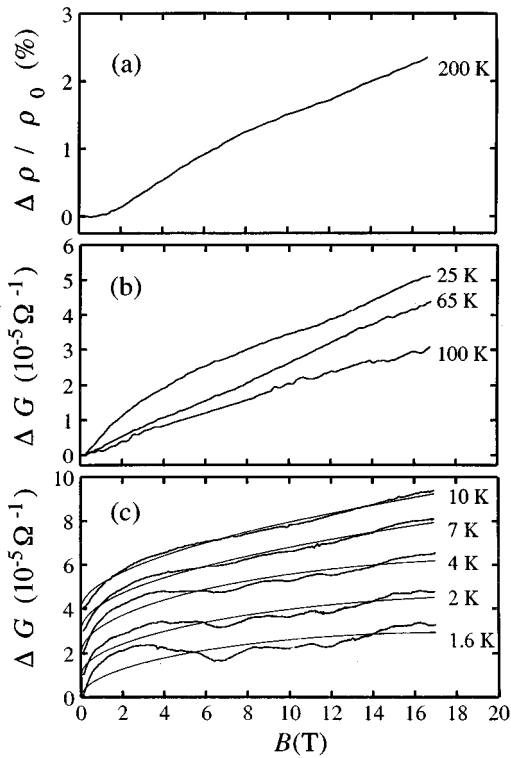


FIG. 4. Temperature variation of magnetotransport parameters for the K-intercalated nanotube bundle showing three distinct temperature regimes: (a) 200 K, (b) 25–100 K, (c) 1.6–25 K. In (c), smooth curves are the best fit to the underlying magnetoconductance described in the text (successive plots are offset by $10^{-5} \Omega^{-1}$ for clarity).

100%: (i) the filling factor for the nanotubes themselves is less than 100%, (ii) nanotubes are hollow, (iii) current does not inject through all of the nanotube walls, and (iv) K intercalation is not homogeneous (unlikely since pristine material is of higher conductance).

Band calculations for closed nanotube structures reveal electronic properties can range from metallic to semiconductor depending on the diameter of the structure and its degree of chirality.¹⁵ The individual nanotubes comprising a bundle are therefore expected to exhibit a range of electronic structure. The low-temperature quantum effects described here are not band transport phenomena, rather they are controlled by the spatial distribution of defects, therefore the electronic structure of individual nanotubes plays no part in their description.

Since the type-II behavior of K-intercalated nanotube bundles is also observed in some pristine nanotube bundles, we assume that charge transfer is low; thus $n \approx 10^{18} \text{ cm}^{-3}$.⁵ With knowledge of f and by assuming a value of $m^* \approx 0.01m_0$ that is typical for turbostratic graphite,¹⁶ we calculate $\tau \approx 10^{-13} \text{ s}$ from the normal component of magnetoconductance determined by curve fitting. From the temperature variation of conductance, Fig. 2, and magnetoconductance, Fig. 4, WL effects collapse at $T \approx 100 \text{ K}$, hence $\tau \approx \tau_{\text{in}} (T = 100 \text{ K})$ or $\tau_{\text{in}} = 4 \times 10^{-13} T^{-0.3} \text{ s}$. From the behavior of $\Delta\sigma_{\text{WL}}$, Figs. 4(b) and 4(c), $\delta \approx 1$ at $T \approx 10 \text{ K}$ and $B \approx 10 \text{ T}$, hence $D \approx 1 \text{ cm}^2 \text{ s}^{-1}$. From these calculated values, $l \approx 5 \text{ nm}$ and at $T \approx 2 \text{ K}$: $l_{\text{in}} \approx 10 \text{ nm}$ and $l_T \approx 20 \text{ nm}$,

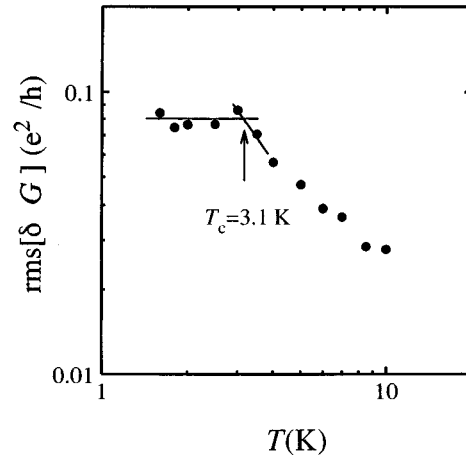


FIG. 5. Temperature variation of the root mean square of conductance fluctuation amplitude measured relative to the smooth curves as in Fig. 4.

where $l_T = \sqrt{\hbar D/k_B T}$ is the thermal diffusion length. This value of l is outside the limit $l \leq 1 \text{ nm}$ imposed above, therefore there is some inaccuracy in the assumptions.

Universal conductance fluctuations (UCF) are often observed in mesoscopic metallic or semiconductor structures and recently in a single multiwall carbon nanotube.^{2,17} The effect is related to the Aharonov-Bohm effect and caused quantum interference of electrons on different trajectories not averaging to zero over a few elastic scattering events. An increase in applied magnetic field shifts the phases of the electrons, therefore a different interference pattern results. Theory predicts sample-specific random fluctuations in conductance as a function of magnetic field with a rms amplitude at $T=0$ of the order e^2/h independent of the sample dimensions or degree of disorder if phase coherence is maintained.¹⁸ Nevertheless it is remarkable that UCF are observed in macroscopic samples since they are usually observed in mesoscopic wires. If phase coherence is not maintained throughout the volume of a macroscopic sample the random magnetoconductance oscillations in any coherent subunits will sum to zero over the sample as a whole. In the cases of pristine type-II and K-intercalated macroscopic nanotube bundles described here, UCF are observed, therefore phase coherence must be maintained in a large part of the sample volume.

The rms amplitude of the UCF was determined from the deviation from fitted smooth curves, Fig. 5. The amplitude is constant below a critical temperature $T_c = 3.1 \text{ K}$, above which it acquires a temperature dependence. Similar behavior, with $T_c = 0.3 \text{ K}$, has been recently reported for a single multiwall carbon nanotube.⁵ If L is the confining dimension, then at temperatures such that L is less than both $l_\phi(T)$ and $l_T(T)$, $\text{rms}[\delta G] = \text{const}$; at higher temperatures when L is greater than both length scales, $\text{rms}[\delta G]$ has the temperature dependence of the shorter of l_ϕ or l_T (here $l_\phi = l_{\text{in}}$; l_{in} and l_T are of the same order so the temperature dependence is not simple).

At T_c , $l_\phi = L$, hence we calculate $L \approx 10 \text{ nm}$ using the calculated expression for τ_{in} and value of D . This is in good agreement with $L \approx 20 \text{ nm}$ determined from UCF for a single multiwall carbon nanotube.²

L corresponds to the mean diameter of the K-intercalated beads of the bead-line pattern, suggesting the defects that prevent the propagation of the K guest atoms along the length of the nanotube also confine electrical charge carriers. The sample is therefore best modeled as a series and parallel combination of units of dimension L with comparable intertube and intratube couplings. The statistical self-averaging of the UCF for each unit yields fluctuations of amplitude $\delta G \approx (e^2/h)(l/L)$ for $L < l_\phi$ or l_T .¹⁹ The observed value of rms $[\delta G] \approx 0.1(e^2/h)$ is in agreement if $l \approx 1$ nm rather than the higher calculated value of $l \approx 5$ nm.

IV. CONCLUSION

Two types of low-temperature magnetotransport behavior in nanotube bundles of helicoidal carbon nanotubes have been observed. Type-I behavior: (i) occurs in the majority of

samples taken from the material deposited on the cathode in the arc discharge process; and (ii) is described by WL and interaction effect in 3D. Type-II behavior: (i) occurs in a minority of samples taken from the cathode and also K-intercalated host material of type I; (ii) exhibits universal conductance fluctuations with $T_c \approx 3$ K; (iii) is described by WL and interaction effect in 3D with an unknown weakly temperature-dependent inelastic scattering mechanism and $l \leq 10$ nm. Since type-II behavior is observed in both K-intercalated and some pristine material, charge transfer is not the dominant effect of intercalation. Rather, K intercalation is accompanied by suppression of conductivity and modification of inelastic scattering processes. This evidence suggests the interaction of guest atoms and host material is fundamentally different in the case of helicoidal carbon nanotubes than that of GICs.

*Present address: Department of Electrical Engineering and Electronics, University of Liverpool, Brownlow Hill, Liverpool L69 3GJ, UK.

¹T. W. Ebbesen, H. J. Lezec, H. Hiura, J. W. Bennet, H. F. Ghaemi, and T. Thio, *Nature (London)* **382**, 54 (1996); H. Dai, E. W. Wong, and C. M. Lieber, *Science* **272**, 523 (1996).

²L. Langer, V. Bayot, E. Grivei, J. -P. Issi, J. P. Heremans, C. H. Olk, L. Stockman, C. Van Haesendonck, and Y. Bruynseraede, *Phys. Rev. Lett.* **76**, 479 (1996).

³V. Z. Mordkovich, M. Baxendale, R. P. H. Chang, and S. Yoshimura, *Carbon* **34**, 1301 (1996).

⁴X. K. Wang, X. W. Lin, V. P. Dravid, J. B. Ketterson, and R. P. H. Chang, *Appl. Phys. Lett.* **62**, 1881 (1993).

⁵S. N. Song, X. K. Wang, R. P. H. Chang, and J. B. Ketterson, *Phys. Rev. Lett.* **72**, 697 (1994).

⁶P. A. Lee and T. V. Ramakrishnan, *Rev. Mod. Phys.* **57**, 287 (1985); G. Bergmann, *Phys. Rep.* **107**, 2 (1984).

⁷M. S. Dresselhaus and G. Dresselhaus, *Adv. Phys.* **30**, 139 (1981).

⁸A. Schmidt, *Z. Phys.* **271**, 251 (1974).

⁹B. L. Al'tshuler, A. G. Aronov, and D. E. Khemel'nitskii, *J. Phys. C* **15**, 7367 (1982).

¹⁰D. E. Beutler and N. Giordano, *Phys. Rev. B* **38**, 8 (1988).

¹¹A. Kawabata, *Solid State Commun.* **34**, 431 (1980); *J. Phys. Soc. Jpn.* **49**, 628 (1980).

¹²See, for example, N. W. Ashcroft and N. D. Mermin, *Solid State Physics* (Holt, Rinehart, and Winston, Philadelphia, 1976).

¹³K. Noto and T. Tsuzuku, *Jpn. J. Appl. Phys.* **14**, 46 (1975).

¹⁴P. A. Lee and T. V. Ramakrishnan, *Phys. Rev. B* **26**, 4009 (1982).

¹⁵R. Saito, R. Fujita, M. S. Dresselhaus, and G. Dresselhaus, *Appl. Phys. Lett.* **60**, 2204 (1992); C. T. White, D. H. Robertson, and J. W. Mintmire, *Phys. Rev. B* **47**, 5485 (1993); R. A. Jishi, M. S. Dresselhaus, and G. Dresselhaus, *ibid.* **48**, 11 385 (1993); Ph. Lambin, L. Phillippe, J. C. Charlier, and J. P. Michenaud, *Comput. Mater. Sci.* **2**, 350 (1994); X. Blase, L. X. Benedict, E. L. Shirley, and S. G. Louie, *Phys. Rev. Lett.* **72**, 1878 (1994).

¹⁶V. Bayot, L. Piraux, J. -P. Michenaud, and J. -P. Issi, *Phys. Rev. B* **40**, 3514 (1989).

¹⁷S. Washburn and R. A. Webb, *Adv. Phys.* **35**, 375 (1986).

¹⁸B. L. Al'tshuler, *Pis'ma Zh. Eksp. Teor. Fiz.* **41**, 530 (1985) [**41**, 648 (1985)]; P. A. Lee and A. D. Stone, *Phys. Rev. Lett.* **55**, 1622 (1985).

¹⁹P. A. Lee, *Physica A* **140**, 169 (1986).